



ROTATING BEAMFORMING METHOD FOR THE USE OF TAILORED GREEN'S FUNCTIONS

Marius Lehmann¹, Daniel Ernst², Carsten Spehr², Marc Schneider¹ and Markus Lummer²

¹ebm-papst Mulfingen GmbH & Co. KG
Bachmühle 2, 74673 Mulfingen, Germany

²German Aerospace Center (DLR)

Abstract

The localization of rotating sound sources using beamforming methods is of interest, for example, in the development of low-noise fans. There are various rotating beamforming methods in the literature, which can be divided into two groups. In the first group, the focus grid is rotated synchronously with the movement of the fan. The steering vectors of the stationary microphones are calculated as a time-dependent function. In the second group, the microphone array is virtually rotated with the fan.

The steering vectors are usually calculated based on the Green's function of a monopole in free field. However, in practical fan applications the sound propagation towards the microphones is often disturbed by obstacles such as the housing of a heat exchanger.

A rotating beamforming method is presented, which considers arbitrary, tailored Green's functions to calculate the steering vectors. In this paper, the Green's functions have been numerically simulated using the Fast Multipole - Boundary Element Method (FM-BEM). The method is validated using both synthetically generated data and data measured in the test rig for a rotating single sound source. Finally, the application on measured data of a fan is shown.

1 INTRODUCTION

The localization of rotating sound sources is of interest in the development of low-noise fans, for example. For this purpose, microphone array measurements can be performed and evaluated using suitable beamforming methods.

There are two groups of beamforming methods in the literature for localizing rotating sound sources. The methods of the first group are based on a co-rotating focus grid. The sound propagation from the rotating focus points to the spatially stationary microphones is time-dependent modeled. An example of a method from the first group is the ROSI algorithm [15, 16].

The methods of the second group use rotating microphones in combination with a rotating focus grid. The sound propagation from the focus points to the microphone positions is therefore time-independent. Because it would be a technical challenge to rotate real microphones at high speeds, the signals from virtually rotating microphones are used. These signals are calculated from the signals of real, stationary microphones. Representatives of this group are the methods of Dougherty et al. [2], Herold & Sarradj [3], Lewis & Joseph [7, 8], Pannert & Maier [12] and Ocker & Pannert [11].

A typical application of an axial fan is to suck air through a heat exchanger. For this purpose, the fan is installed in a housing together with the heat exchanger. This can influence the inflow to the fan and therefore also the aeroacoustic sound generation. It is thus of interest to investigate such an installation situation with beamforming methods when developing fans.

However, the above-mentioned rotating beamforming methods can only take into account sound propagation under acoustic free-field conditions or rotationally symmetrical propagation conditions. However, the housings of heat exchangers are usually not rotationally symmetrical. The authors of this paper have therefore developed a method that can use arbitrary, tailored Green's functions to calculate the steering vectors for rotating beamforming. This so-called RoBeaT method (Rotating Beamforming using Tailored Green's functions) was first presented in [6]. In [5] it was then also used for sound source localization on fans.

In this contribution, the method will be presented again and its application demonstrated and discussed. The basics of the method are presented in section 2. Afterwards, setups for validation are shown in section 3. The method is then validated in section 4. In section 5, the application on measurement data of a fan is shown. The results are summarized in section 6.

2 BEAMFORMING METHODS

In this section, some basics about beamforming are given first and then the RoBeaT method is presented.

2.1 Frequency domain beamforming using cross spectra

A widely used procedure for processing microphone array data using beamforming methods is to compute the auto and cross power spectra of the microphone data and store them in the so-called *cross-spectral matrix*, CSM) \mathbf{C} :

$$\mathbf{C} = \mathbf{E} \left(\frac{1}{2} \hat{\mathbf{p}} \hat{\mathbf{p}}^* \right) \in \mathbb{C}^{M \times M} \quad (1)$$

where \mathbf{E} is the expectation operator, $\hat{\mathbf{p}}$ is the M -dimensional vector of complex pressure amplitudes and M is the number of microphones. To calculate the auto power spectra of the source strengths A at the focus points, the cross spectral matrix \mathbf{C} is multiplied by the so-called steering vectors $\hat{\mathbf{w}}$, the weighted Green's functions \hat{g}_m .

$$A = \hat{\mathbf{w}}^* \mathbf{C} \hat{\mathbf{w}} \quad (2)$$

Depending on the source model and propagation conditions, the Green's functions provide the complex pressure amplitudes that would be induced at the microphone positions by a unit source

at the focus point. The simplest approach is to use the free-field Green's function of a monopole. The Green's function \hat{g}_m between a certain focus point \mathbf{y} and a microphone m at location \mathbf{x}_m is then:

$$\hat{g}_m = \frac{1}{r_m} e^{-jkr_m}, \quad r_m = \|\mathbf{y} - \mathbf{x}_m\|_2 \quad (3)$$

Steering vector formulations

There are various ways of weighting Green's functions in order to calculate the so-called *Steering vectors*. Sarradj [13] gives an overview of the most frequently used formulations. The first and third of these formulations are used in this paper:

Formulation I: The simplest approach is to correct only the phase of the microphone signals. As a result, the maximum of the beamforming map corresponds to the source position. However, the source strength is not reconstructed:

$$\hat{w}_m^I = \frac{1}{M} \frac{\hat{g}_m}{|\hat{g}_m|} \quad (4)$$

Formulation III: The third steering vector formulation is based on a minimization approach. The difference between the vector of the measured microphone amplitudes and the product of the complex source amplitudes and the Green's functions is minimized. The resulting steering vector formulation \hat{w}_m^{III} is:

$$\hat{w}_m^{III} = \frac{\hat{g}_m}{\|\hat{\mathbf{g}}\|_2^2} \quad (5)$$

The source strength at the source position is reconstructed correctly, but the source position is not.

Point spread function

Beamforming results depend on both the spatial microphone arrangement and the steering vectors. The influence of these two parameters on the beamforming map of a single sound source is described by the *Point Spread Function* (PSF). It is the spatial impulse response to a unit point source at a specific focus point \mathbf{y}_s . The CSM induced by the point source can be calculated as follows:

$$\mathbf{C}_s = \hat{\mathbf{g}}(\mathbf{y}_s) \hat{\mathbf{g}}(\mathbf{y}_s)^* \quad (6)$$

This results in the source strength at a focus point \mathbf{y} :

$$A^{\text{PSF}}(\mathbf{y}) = \hat{\mathbf{w}}(\mathbf{y})^* \mathbf{C}_s \hat{\mathbf{w}}(\mathbf{y}) = \hat{\mathbf{w}}(\mathbf{y})^* \hat{\mathbf{g}}(\mathbf{y}_s) \hat{\mathbf{g}}(\mathbf{y}_s)^* \hat{\mathbf{w}}(\mathbf{y}) = |\hat{\mathbf{w}}(\mathbf{y})^* \hat{\mathbf{g}}(\mathbf{y}_s)| \quad (7)$$

2.2 Beamforming Method using tailored Green's functions (RoBeaT)

The RoBeaT method has been developed to consider real propagation conditions in localization of rotating sound sources. It is described below based on [6] and [5].

The workflow of the RoBeaT method is shown in Figure 1. The method can be used for stationary beamforming in the frequency domain as well as for stationary and rotating beamforming in the time domain.

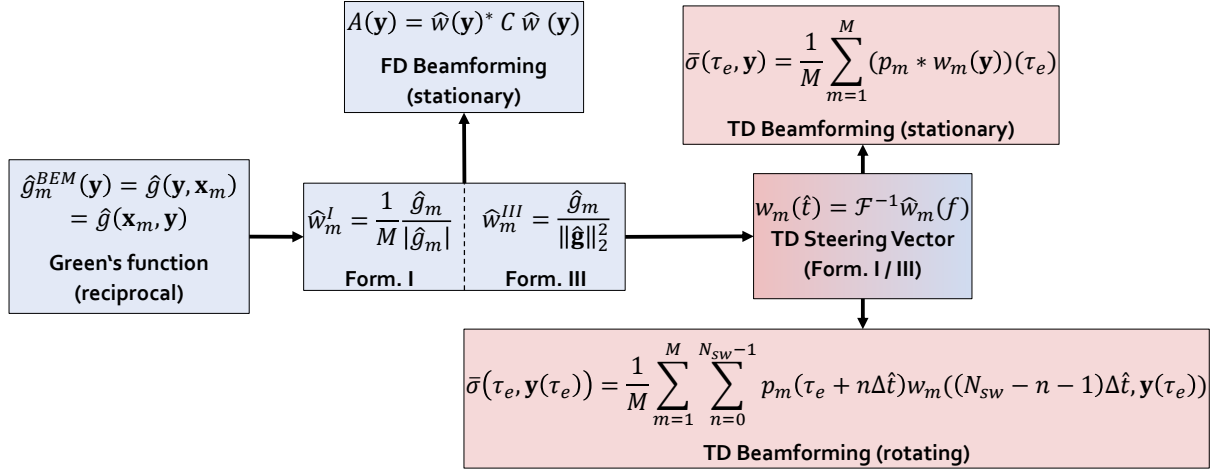


Figure 1: Flow chart of RoBeaT [5].

Steering vector calculation in the frequency domain

The RoBeaT method uses arbitrary Green's functions which have been determined in the frequency domain as input. In the present work, the tailored Green's functions are determined by boundary element simulation (BEM). To reduce the number of simulations required, the source (focus point \mathbf{y}) and receiver (microphone \mathbf{x}_m) are reversed.

$$\hat{g}(\mathbf{y}, \mathbf{x}_m) = \hat{g}(\mathbf{x}_m, \mathbf{y}) \quad (8)$$

The steering vectors are calculated from these through weighting using eq. 4 or 5. In the stationary reference system, these steering vectors can be used directly for beamforming in the frequency domain based on cross spectra (eq. 2).

Transformation of the steering vectors into the time domain

For sound source localization in the rotating reference frame, a rotating focus grid and the signals of spatially stationary microphones are used. As already mentioned in the introduction, the sound propagation between the focus grid and the microphones is time-dependent. Beamforming is therefore performed in the time domain.

To calculate the steering vectors in the time domain, the first step is to calculate the Green's functions in a specific frequency range $f_{\min}^{\text{BEM}} \leq f^{\text{BEM}} \leq f_{\max}^{\text{BEM}}$ at a delta of Δf^{BEM} . Subsequently, the steering vectors $\hat{w}_m^{\text{BEM}}(f)$ are calculated according to formulation I or III (eq. 4 or 5). The Green's functions only need to be determined up to the highest frequency of interest for beamforming. If the highest calculated frequency f_{\max}^{BEM} is less than half the sampling rate of the measurement $f_s/2$, the remaining entries in the frequency spectrum of the steering vectors are set to zero.

The spectrum of the steering vectors is then transformed into the time domain using inverse Fast Fourier Transformation (iFFT). To determine the negative frequencies, it is first conjugated

and complex mirrored.

$$w_m(\hat{t}) = \mathcal{F}^{-1} \hat{w}_m(f) \quad (9)$$

with $-f_s/2 < f < f_s/2$. In this paper, the result is referred to as the weighted impulse response in the time domain and consists of $N_{\text{sw}} = f_s/\Delta f^{\text{BEM}} + 1$ sampling points. \hat{t} is the time related to the weighted impulse response and differs from the global time t .

Time domain beamforming

The time signals of the source strength at the focus points $\bar{\sigma}(\tau_e, \mathbf{y}(\tau_e))$ are calculated time step by time step from the measured microphone signals. For each individual time step, the weighted impulse responses are multiplied by the corresponding sections from the microphone signals and the resulting time signals are summed up. For a stationary focus grid, this procedure corresponds to a convolution of the microphone signals p_m with the corresponding weighted impulse responses $w_m(\hat{t}, \mathbf{y})$ from the microphones m to the stationary focus points $\mathbf{y}(\tau_e) = \mathbf{y}$:

$$\bar{\sigma}(\tau_e, \mathbf{y}) = \frac{1}{M} \sum_{m=1}^M (p_m * w_m(\mathbf{y}))(\tau_e) \quad (10)$$

A co-rotating focus grid is used to localize rotating sound sources. This causes the weighted impulse responses $w_m(\hat{t}, \mathbf{y}(\tau_e))$ to become dependent on the source time τ_e . To determine the weighted impulse responses at a specific source time, the positions $\mathbf{y}(\tau_e)$ of the rotating focus points are calculated first. The weighted impulse responses $w_m(\hat{t}, \mathbf{y}(\tau_e))$ are then determined from the stationary, weighted impulse responses using spatial *nearest neighbor* interpolation. The stationary, weighted impulse responses are therefore used as a *look-up table*.

Due to the dependence of the weighted impulse responses on the evaluation time, it is, in contrast to the stationary case, not possible to calculate the time signals of the source strengths $\bar{\sigma}(\tau_e, \mathbf{y}(\tau_e))$ at the rotating focus points by convolution of the microphone signals with the weighted impulse responses. Instead, to calculate the rotating time signals at a specific time τ_e , the associated time segments of the microphone signals $p_m(\tau_e + n\Delta\hat{t})$ must be multiplied by the weighted impulse responses $w_m(\hat{t}, \mathbf{y}(\tau_e))$ of the focus positions $\mathbf{y}(\tau_e)$ and the products are added up.

$$\bar{\sigma}(\tau_e, \mathbf{y}(\tau_e)) = \frac{1}{M} \sum_{m=1}^M \sum_{n=0}^{N_{\text{sw}}-1} p_m(\tau_e + n\Delta\hat{t}) w_m((N_{\text{sw}} - n - 1)\Delta\hat{t}, \mathbf{y}(\tau_e)) \quad (11)$$

In eq. 11, $\Delta\hat{t} = \frac{1}{f_s}$ is the inverse of the sampling frequency f_s and N_{sw} is the number of sample points in the weighted impulse responses.

3 VALIDATION SETUP

This section presents the test cases for validating the RoBeaT algorithm.

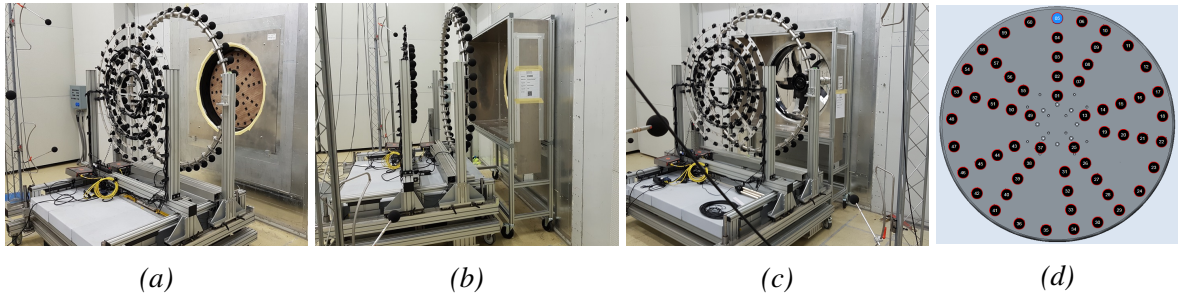


Figure 2: Setup of the validation experiments with reference sound source or fan and microphone array in the fan test bench. (a) Without box. (b) With box. (c) Fan with box. (d) Numbering of the loudspeakers. Loudspeaker no. 5 (marked in blue) was used for the measurements in this study.

3.1 Measurement setup

The measurement setups for validating the RoBeaT method are shown in fig. 2. The basic idea is to use a typical test setup in a fan test bench and to replace the fan with a known sound source in the first step.

The measurements in this paper have been done in the aeroacoustic fan test rig of ebm-papst Mulfingen GmbH & Co. KG. This is divided into two semi-anechoic chambers separated by a wall. In a typical measurement setup of an axial fan, it is installed in a so-called wall ring in the separating wall. A wall ring with an inner diameter of $d = 0.96\text{m}$ is used. To model the influence of the housing of a heat exchanger, a rectangular box is used (Figure 2b). This has the dimensions $1.54 \times 1.14 \times 0.46\text{m}^3$.

The sound signals are recorded with a microphone array. The sound propagation is simulated by boundary element method in the form of tailored Green's functions and used to calculate the steering vectors.

3.2 Reference sound source

For the experiments with a known sound source, a disk with speakers is used, which was developed by Sauereßig in [14] (Figure 2d). The diameter of the disk corresponds to the diameter $d = 0.952\text{m}$ of the axial fan, which will be investigated later. The disk is mounted on an electric motor so that the speakers can be measured both stationary and rotating. In this paper, measurements are done with a rotational speed of $n = 230\text{rpm}$.

The front of the reference sound source is positioned at a distance of $\Delta z = 0.18\text{m}$ from the front edge of the wall ring. This is to take into account the aspect that the sound also propagates out of the wall ring in a real setup with a fan.

Only one speaker is used in this study (marked blue in (Figure 2d)). The input signal is bandpass filtered white noise between $f = 0.5\text{kHz}$ and $f = 10\text{kHz}$.

3.3 Microphone array

The microphone array used for the measurements in this paper can be seen in Figure 2a to 2c. It consists of a total of $M = 80$ microphones, which are divided into three ring arrays with $M_1 = 40$,

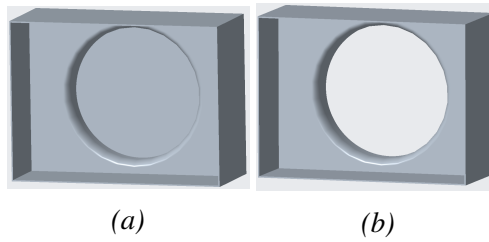


Figure 3: CAD models for generating the computational meshes for the FM-BEM simulations. (a) Box with closed wall ring. (b) Box with open wall ring.

$M_2 = 24$ and $M_3 = 16$ microphones. The rings have the diameters $d_1 = 1.6$ m, $d_2 = 0.8$ m and $d_3 = 0.4$ m. The second and third rings are arranged on the same plane. The distance to the front edge of the wall ring is $\Delta z = 0.8$ m for the large microphone ring and $\Delta z = 1.3$ m for the two small microphone rings. In this paper, the microphones of the smallest ring are not used.

The data acquisition system is an I²S front end from CAE Software and Systems GmbH [1] with the corresponding digital MEMS microphones. The time signals are recorded for 15 seconds at a sampling rate of $f_s = 48077$ Hz and then resampled to a sampling rate of $f_s = 24000$ Hz.

3.4 Simulation setup

The tailored Green's functions are calculated numerically using the *Boundary Element Method* (BEM). For this purpose, the *Fast Multipole-Boundary Element Method* (FM-BEM) code *FMCAS* [9, 10] is used.

Only the box-shaped housing of the heat exchanger, the separating wall and the wall ring are taken into account in the simulations. To model the rotating loudspeaker disk, the wall ring is closed at the axial position where the front of the disk is located in the experimental setup. For the evaluation of the fan measurements, however, the simulations are carried out with the wall ring open. Fig. 3a shows a CAD model with a closed wall ring and fig. 3b with an open wall ring. FMCAS generates the computational meshes based on these models.

The simulations are run in the frequency range between $f_{\min}^{\text{BEM}} = 60$ Hz and $f_{\max}^{\text{BEM}} = 4500$ Hz. The distance between two frequencies is $\Delta f^{\text{BEM}} = 60$ Hz. In order to be able to calculate the steering vectors in the time domain using iFFT, the entries in the frequency spectrum of the steering vectors in the range between $f_{\max}^{\text{BEM}} = 4500$ Hz and $f_s/2 = 12000$ Hz are set to zero.

The Green's functions are calculated on two-dimensional, square grids. These have the dimensions 1.44×1.44 m². The distance between two grid points is $\Delta y = 0.01$ m. For test cases with the reference sound source, the grid points are placed on the front of the disk. For the calculation of spatially stationary point spread functions in the frequency domain according to eq. 7, these grid points are used directly as focus points. For rotating beamforming, the stationary, weighted impulse responses are first calculated on the evaluation grid of the BEM simulations. The rotating, weighted impulse responses at the rotating focus points are then determined for each time step by *nearest neighbor* interpolation. In the case of the fan, a three-dimensional focus grid adapted to the blades is used. As a basis for this, the spatially stationary Green's functions are evaluated on several circular, two-dimensional planes in the axial direction.

3.5 Evaluation criteria

In this paper, beamforming maps are used to compare different beamforming methods. To make the results better comparable, two evaluation criteria based on Sarradj [13] are used.

The first criterion describes the **deviation** of the indicated source level L_s at the source position \mathbf{y}_s **from the true level** L_e :

$$\Delta L_s = L_e - L_s \quad (12)$$

The true level of the loudspeaker in the reference sound source is determined in this paper by sound power measurement. The process is described in [5]. The sound power level is determined for the setup without box in the fan test bench in accordance with standard ISO 13347-3 [4].

The second criterion evaluates the **spatial deviation** of the maximum of the beamforming map **from the actual source position**:

$$\Delta y = \|\mathbf{y}_{\max} - \mathbf{y}_s\|_2 \quad (13)$$

4 VALIDATION WITH KNOWN SOUND SOURCES

In this section, the RoBeaT method will be validated. For this purpose, spatially stationary, synthetically generated point spread functions are first discussed and then measurement data from the rotating reference sound source are evaluated.

4.1 Results from synthetic data with stationary source

The synthetic validation of the RoBeaT method in the frequency domain is based on point spread functions (PSF). For these, the actual source position and level is known. The PSFs are calculated using eq. 7. Six different cases are compared in which the calculation of the CSM and the steering vectors is varied. Only one source position is considered at $x = 0.47$ m, $y = 0$ m and $z = 0.18$ m. The model with the wall ring closed at $z = 0.18$ m (Figure 3a) is used for the BEM simulations.

An overview of the test cases evaluated is given in table 1. In the first two cases, simulated measurement data based on the free-field Green's functions (eq. 3) is used. No geometry is therefore taken into account. The steering vectors are also calculated based on the free-field Green's functions. Both formulations (I and III, eq. 4 and eq. 5) are used. These cases serve as a reference and show the properties of the microphone array used under ideal conditions.

In the other four cases, measurement data for the geometry with box and wall ring is simulated. For this purpose, the tailored Green's functions calculated by BEM are used to model the sound propagation between the source position and the microphone positions for this case. Beamforming is performed both under free-field assumption and taking the geometry into account. The steering vectors are calculated according to both formulation I (eq. 4) and formulation III (eq. 5).

On the one hand, these four cases are used to show the influence of the presence of the box and the wall ring on the results of the free-field beamformer. On the other hand, it will be investigated to what extent this influence can be compensated by considering the tailored Green's functions.

No.	CSM calculation	Steering vector calculation	Formulation
1	Without geometry	Freefield	I
2	Without geometry	Freefield	III
3	With geometry	Freefield	I
4	With geometry	Freefield	III
5	With geometry	Tailored	I
6	With geometry	Tailored	III

Table 1: Overview of the test cases for validating the RoBeaT method with stationary, synthetic measurement data.

Beamforming maps

First, the beamforming maps for the third-octave band center frequencies $f = 630\text{Hz}$, $f = 1000\text{Hz}$, $f = 2500\text{Hz}$ and $f = 4000\text{Hz}$ are compared in fig. 4. The color range of each beamforming map is adapted to its respective maximum within the wall ring (black circle).

The beamforming maps of the first two cases with free-field CSM and free-field steering vectors scale with the frequency. The round main lobe is centered at the source position and becomes narrower with increasing frequency. It is surrounded by circular side lobes, which are arranged concentrically around the source position and have a constant level in the circumferential direction. Their diameter also decreases with frequency. Starting at $f = 1000\text{Hz}$, the strongest side lobe is located within the wall ring. The formulation of the steering vector (I or III) has no visible influence.

For the cases where the CSM was calculated based on the tailored Green's functions to consider the geometry, but the steering vectors were calculated based on free-field Green's functions, there is also almost no dependence on the steering vector formulation (lines 3 and 4). In contrast to the first two cases, however, the levels of the side lobes are not constant in the circumferential direction. Although circular side lobes can also be recognized, especially at $f = 2500\text{Hz}$ and $f = 4000\text{Hz}$, their level is strongly dependent on the circumferential angle. The strongest side lobes are located at the same positions as in the cases with free-field CSM. However, the levels at the focus points outside the main lobe are higher than in these cases.

The fifth and sixth rows show the results for the cases in which the tailored Green's functions have been considered both in the calculation of the CSM and in the calculation of the steering vectors. The main lobe widths are visibly reduced, even compared to the cases without geometry. The levels at the focus points outside the main lobe are reduced, especially from $f \geq 1000\text{Hz}$ compared to the cases with geometry and free-field evaluation. In contrast to the cases with free-field steering vectors, there is a dependence on the steering vector formulation. For formulation III, the maximum of the main lobe does not coincide with the source position, especially at low frequencies. Furthermore, higher levels are found at all focus points outside the wall ring than inside the wall ring.

Deviation from the true level

The frequency-dependent deviation from the true level is shown in fig. 5a. As shown in [13], formulation III has to be used to reconstruct the source level correctly. The results calculated

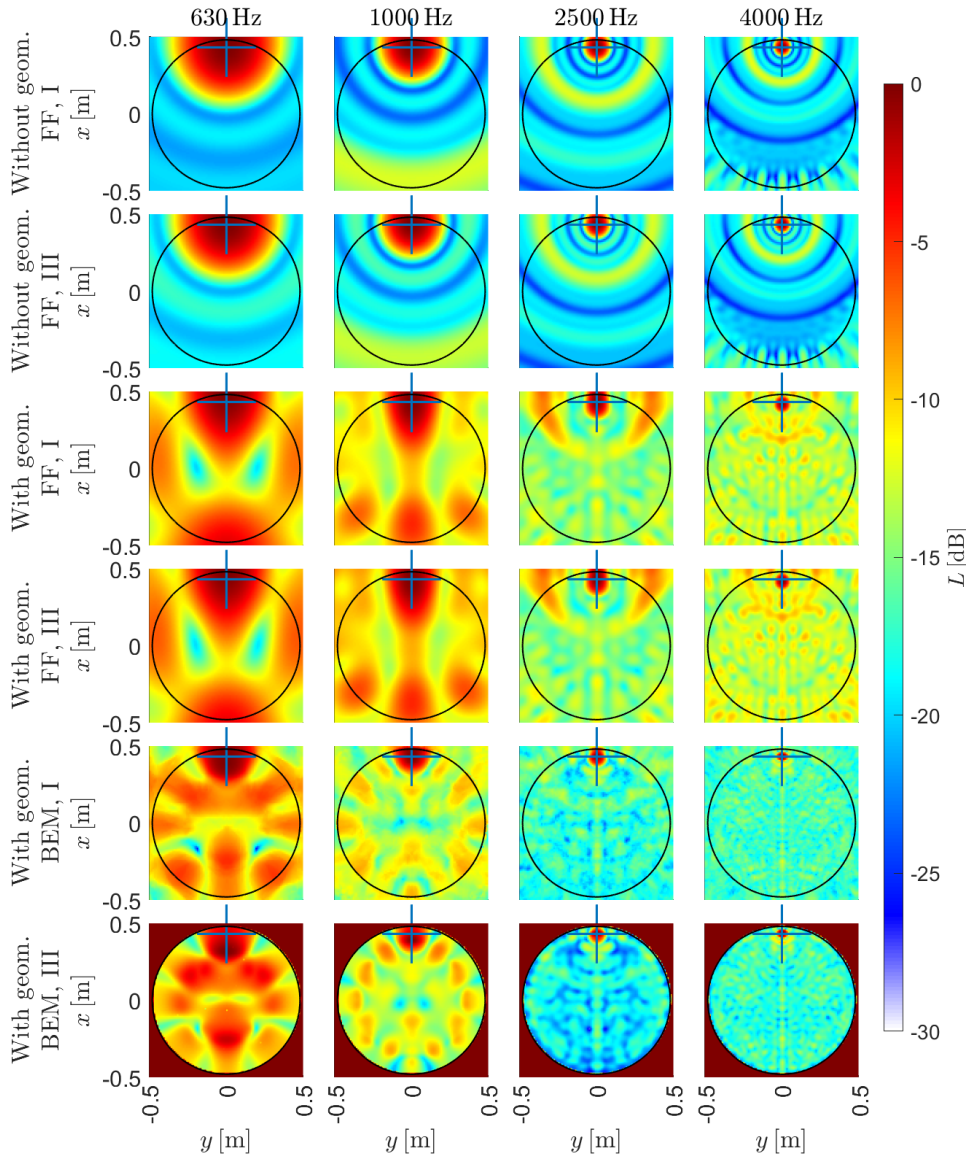


Figure 4: Point spread functions of a stationary source to validate the RoBeaT method in the frequency domain with synthetic data. Variation of CSM (without geometry/ with geometry), steering vector calculation (from free field (FF)/ with tailored Green's functions from BEM) and formulation (I or III).

using formulation III will therefore be presented first. In these cases, the true level is exactly found if the same Green's functions are used to calculate the steering vectors as to calculate the CSM (second and sixth case). The solid blue curve lies behind the solid yellow curve and is therefore not visible. However, the source level is not found when the CSM on the basis of the tailored Green's functions is evaluated with free-field beamforming. The deviation is frequency-dependent in the range $-4\text{ dB} < \Delta L_s < 4\text{ dB}$.

As shown in [13], formulation I does not necessarily reconstruct the true level correctly. In

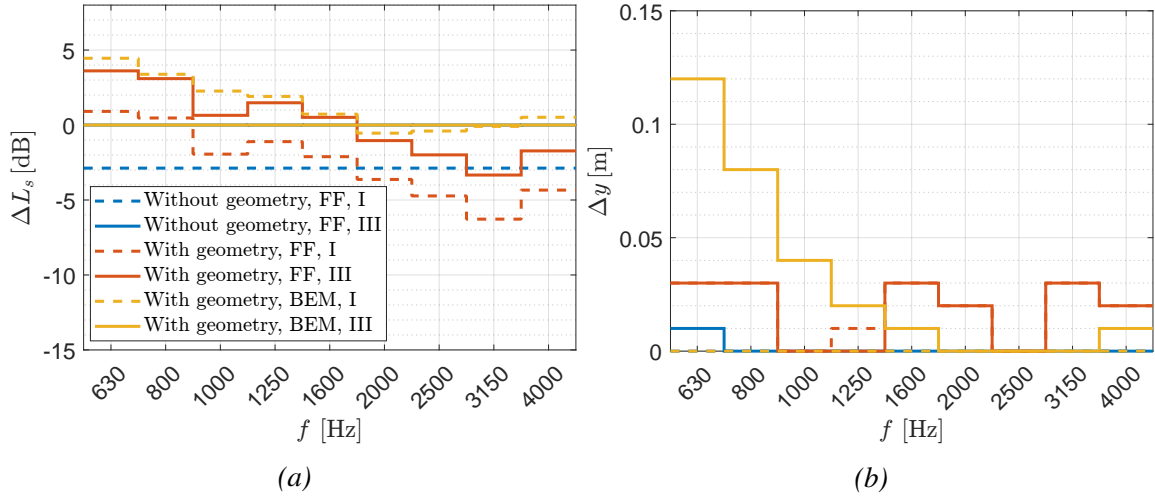


Figure 5: Validation of the RoBeaT method in the frequency domain with synthetic data. Variation of CSM (without geometry/with geometry), steering vector calculation (from free field (FF)/with tailored Green’s functions from BEM) and formulation (I or III). Evaluation criteria over frequency: (a) deviation from source level, (b) deviation from source position.

the first case, the deviation is independent of the frequency and is $\Delta L_s \approx -3$ dB. In the other case with free-field steering vectors (case 3), the deviation from the corresponding result with formulation III (case 4) is similarly large. However, it is slightly frequency-dependent and lies between $2.5 \text{ dB} < \Delta \Delta L_s^{\text{III-I}} < 3$ dB. For the fifth case, which is based purely on the tailored Green’s functions, the overall deviation is highest at $f = 630$ Hz with $\Delta L_s \approx 4.5$ dB. However, it decreases with increasing frequency and is even lower from $f = 2000$ Hz than in the fourth case with identical CSM and free-field beamforming using formulation III.

Spatial deviation from the actual source position

The spatial deviation from the actual source position is shown in fig. 5b. First of all, it can be seen that the source position is found exactly with steering vector formulation I if the correct Green’s functions are used to calculate the respective steering vectors. However, there are slight deviations when the CSM is calculated based on the tailored Green’s functions and the steering vectors are calculated based on the free-field Green’s functions.

Even with formulation III, the actual source position is partially found correctly. This applies especially to the pure free-field case. For the case with CSM taking the geometry into account, the results of the free-field beamformer deviate from the actual source position for most frequencies.

The largest errors occur when the tailored Green’s functions are used to calculate both the CSM and the steering vectors according to formulation III. The spatial deviation is largest at $f = 630$ Hz with $\Delta y = 0.12$ m and decreases continuously with increasing frequency. At $f = 2500$ Hz and $f = 3150$ Hz, the calculated and actual source position match. At $f = 4000$ Hz there is another slight deviation ($\Delta y = 0.01$ m).

Summary and discussion of the results

In this section, the measurement data has been generated synthetically in order to test the RoBeaT method under controlled conditions.

It has become clear that the results of free-field beamforming are noticeably influenced if the geometry is taken into account when calculating the CSM. However, the results of the free-field beamformer show only slight dependence on the steering vector formulation (I or III).

If the geometry is also taken into account when calculating the steering vectors, the results are improved. Depending on the steering vector formulation, the source level and source position are matched exactly. However, the beamforming maps do not correspond to those of the first two cases, where only free-field Green's functions were used.

Furthermore, the results are significantly more dependent on the steering vector formulation than with free-field beamforming. With formulation I, these are improved for all frequencies. With formulation III, on the other hand, better results are only achieved in the mid and upper frequency range. In some cases, these are even slightly better than with formulation I. In the lower frequency range, however, the results based on Formulation III are characterized by the fact that the position of the sound source is not found correctly.

The investigations in this section have shown that the RoBeaT method provides correct results. However, the results obtained by this approach are not identical to those obtained under pure free-field conditions. One possible explanation for this is that the tailored Green's functions take reflections, diffraction and shadowing into account in addition to direct sound propagation. The consideration of reflections can be seen analogously as the addition of further virtual microphones. The diffraction and shadowing of the sound on the geometry changes the propagation times of the sound and the amplitudes of the Green's functions between the source and the microphones. This can be interpreted as a virtual modification of the position and weighting of the physical microphones.

4.2 Results from measured data with rotating source

In this section, data measured with the setup described in section 3.1 to 3.3 with rotating reference sound source is evaluated. The implementation of the RoBeaT algorithm with rotating focus grid described in section 2.2 was used for the evaluation. In the previous section, it was shown that the results of the free-field steering vectors are almost independent of the steering vector formulation. For this reason, only the results for one steering vector formulation are shown below for these cases.

When comparing the results with the results from the previous section, it should be borne in mind that there are two major differences between the setups: Firstly, the microphone data was not generated synthetically, but with a real measurement setup. However, the steering vectors will again be calculated synthetically (free field or BEM). On the other hand, the measurement data in this section was generated with a rotating sound source.

Beamforming maps

The beamforming maps are shown in Fig. 6. In the first case with measurement without rectangular box and evaluation with free-field steering vectors, the levels at the focus points outside

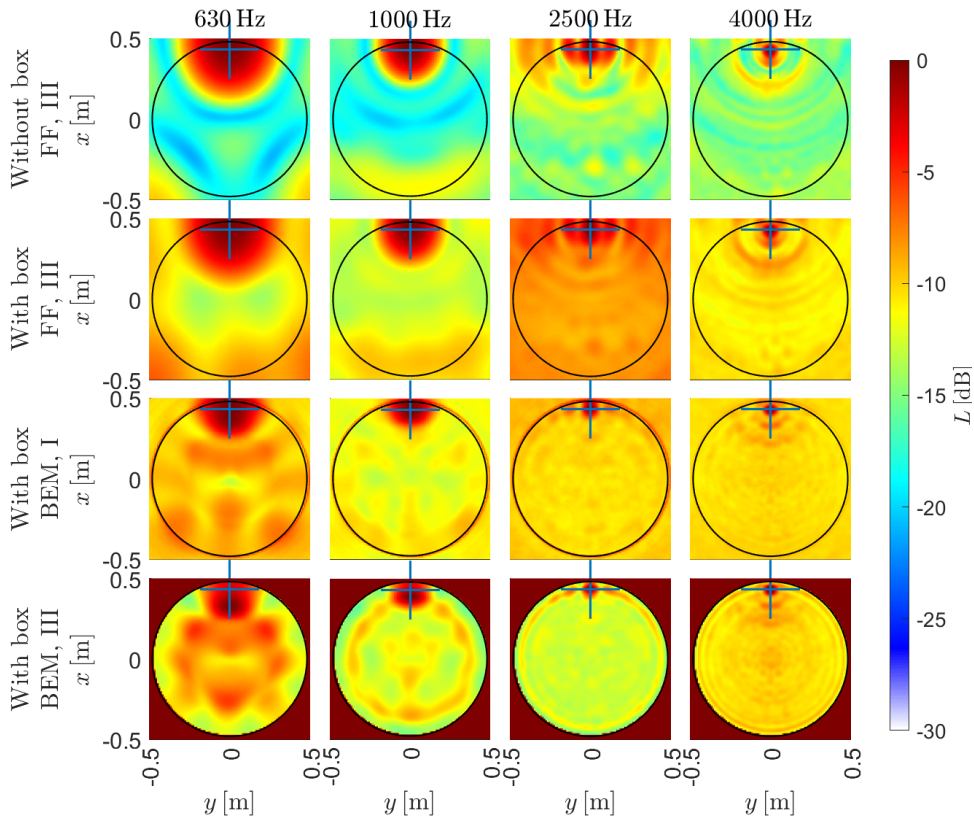


Figure 6: Beamforming maps for validation of the RoBeaT method in the time domain with data measured in the test bench with rotating reference sound source ($n = 230$ rpm). Single loudspeaker (no. 5) with white noise. Variation of setup (without box/with box), steering vector calculation (from free field (FF)/ with tailored Green's functions from BEM) and formulation (I or III).

the main lobes are higher than in the corresponding synthetic cases without geometry. Furthermore, additional side lobes occur near the source position at $f = 2500$ Hz.

These findings also apply to the second case with box and free-field steering vectors. However, the levels are spatially much more evenly distributed than in the corresponding synthetic case with a spatially stationary source.

As with the synthetic cases, the main lobes become narrower when the box measurement is evaluated with beamforming based on the tailored Green's functions. The levels outside the main lobes are always higher than in the corresponding synthetic cases. Furthermore, as in the synthetic case, the position of the main lobes in the low frequency range deviates from the actual source position when using Steering Vector Formulation III.

Deviation from the true level

The deviations of the various source levels calculated by beamforming from the true level are shown in fig. 7a. As described in section 3.5, the true level was determined from the sound power level of the measurement setup without a box.

The deviations from the true level are smallest when the tailored Green's functions are used to calculate the steering vectors using Formulation III. The deviation is in the range $-2\text{ dB} < \Delta L_s < 2\text{ dB}$ for all frequencies. In contrast to this, the results for free-field beamforming (both for the measurement without box and the measurement with box) are only at $f = 2500\text{ Hz}$ and $f = 3150\text{ Hz}$ in this range. Too high levels are calculated in all other frequency bands. The highest deviation occurs for both measurements at $f = 1250\text{ Hz}$ and is $\Delta L_s \approx 6.8\text{ dB}$ for the case without box and $\Delta L_s \approx 6.4\text{ dB}$ for the case with box.

Even when using Formulation I to calculate the steering vectors based on the tailored Green's functions, the deviations for all frequencies except $f = 2500\text{ Hz}$ and $f = 3150\text{ Hz}$ are lower than with free-field steering vectors under Formulation III. For $f = 2000\text{ Hz}$ and $f = 4000\text{ Hz}$, it is lower than in all other cases.

Spatial deviation from the actual source position

The spatial deviation from the actual source position is shown in fig. 7b. For the evaluation of the measurement without box with free-field beamforming, the deviations are $\Delta y < 0.025\text{ m}$ below $f = 2500\text{ Hz}$ and $\Delta y < 0.015\text{ m}$ from $f = 2500\text{ Hz}$. However, the source position is never met exactly.

In the results of the measurement with box and free-field beamforming, $\Delta y = 0\text{ m}$ is found at $f = 1000\text{ Hz}$. For the other frequencies, $\Delta y < 0.025\text{ m}$ applies as for the measurement without a box. However, in contrast to the results of the measurement without a box, there is no trend for the deviation to become smaller at higher frequencies.

The source position is exactly found in the results based on the tailored Green's functions under Formulation I in three frequency bands. In five frequency bands, the spatial deviation for this case is lower than in the cases with free-field beamforming. It only reaches its maximum $\Delta y = 0.02\text{ m}$ in one frequency band (at $f = 630\text{ Hz}$). In all other frequency bands it is below $\Delta y = 0.01\text{ m}$.

As in the corresponding synthetic, stationary case, the deviations with steering vector formulation III and tailored Green's functions are greater in the lower frequency range $f < 1250\text{ Hz}$ than in all other cases ($0.05\text{ m} \leq \Delta y_{\text{max}} \leq 0.11\text{ m}$). In the upper frequency range $f \geq 1250\text{ Hz}$, the deviations are in the same range $\Delta y < 0.025\text{ m}$ as in the other cases.

Summary and discussion of the results

From the results shown, it is clear that the RoBeaT method can also be applied to rotating sound source localization from measured data using the tailored Green's functions simulated in the stationary frequency domain. The source level of the loudspeaker is reconstructed with greater accuracy than when using free-field Green's functions.

The source position is also well matched with Formulation I. However, as in the previous section, the deviation for Formulation III is very high in the lower frequency range.

In the results with steering vectors from tailored Green's functions, the main lobes are narrower at low frequencies. This can be explained by the fact that reflections are used as additional information by means of the tailored Green's functions. As explained, the addition of further virtual microphones to the existing microphone array can be seen as an analogy.

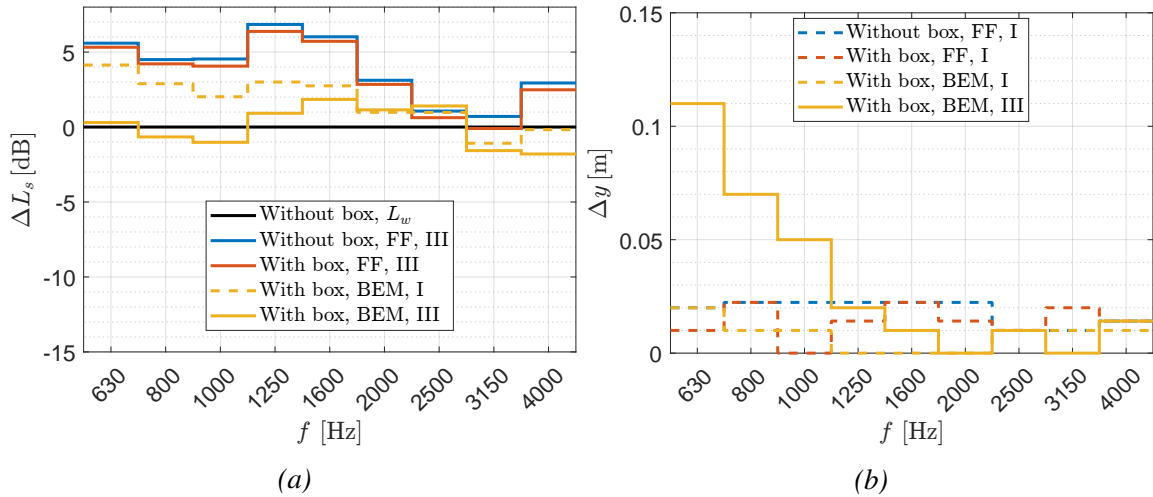


Figure 7: Validation of the RoBeaT method in the time domain with data measured in the test bench with rotating reference sound source ($n = 230$ rpm). Single loudspeaker (no. 5) with white noise. Variation of setup (without box/ with box), steering vector calculation (from free field (FF)/ with tailored Green’s functions from BEM) and formulation (I or III). (a) Deviation from the source level, (b) Deviation from the source position.

5 APPLICATION ON MEASUREMENT DATA OF A FAN

In this section, the RoBeaT method is applied to measurement data from a fan. The measurement setup is shown in fig. 2c. It corresponds to the measurement setup from the previous section with the only difference that the rotating loudspeaker disk has been replaced by an axial fan with identical diameter. The fan rotates clockwise at a speed of $n = 929$ rpm. The operating point without static pressure increase is examined. In this paper, only results for the measurement with box and evaluation with RoBeaT (free field and tailored Green’s functions) are shown. For further results, please refer to [5].

5.1 Beamforming maps

The beamforming maps in fig. 8 are calculated on body-adapted focus grids, as described in section 3.4. These are adapted to the suction-side surface of the fan blades. The rotating impulse responses on this focus grid are calculated for each time step by three-dimensional nearest neighbor interpolation from stationary impulse responses on a cylindrical grid. Based on the findings from the previous section, formulation I is used to calculate the steering vectors.

For the first case with free-field steering vectors, the dynamics of the beamforming map are very low at $f = 630$ Hz. At $f = 1000$ Hz, the highest levels are found in the outer third of the leading edges. The dynamic range is also significantly greater ($\Delta L < 8$ dB).

In the second case with tailored Green’s functions, the maximum level difference in the beamforming map at $f = 630$ Hz is increased compared to the first case ($\Delta L \approx 5$ dB). This clearly identifies the leading edges as the areas with the highest sound radiation. Also at $f = 1000$ Hz, the areas of the maximum levels are more clearly identified when using tailored Green’s functions. However, the maximum level difference within the map is lower than in the freefield case

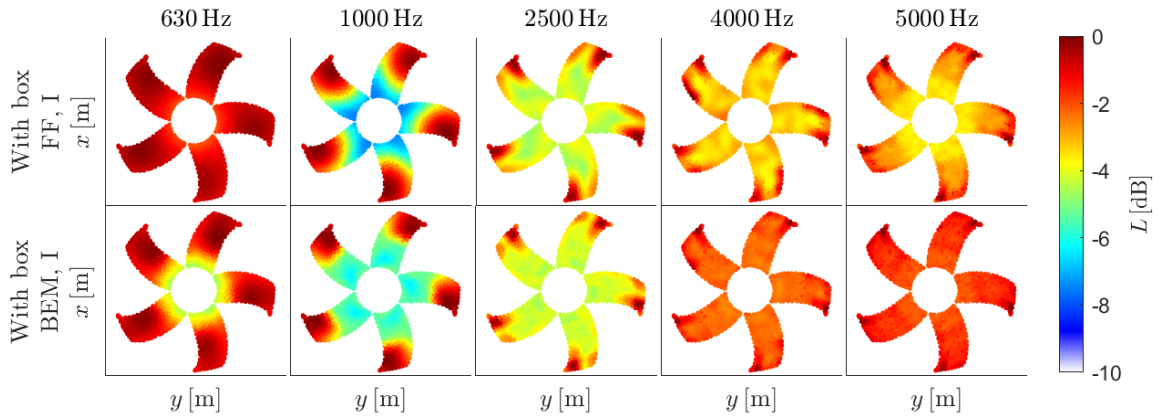


Figure 8: 3D beamforming maps for measurement with fan in box. Comparison between the results of free-field Green's functions (FF) and tailored Green's functions. Steering vector formulation I. The fan rotates clockwise.

($\Delta L < 6$ dB).

For $f = 2500$ Hz, the results of the two cases are similar. However, the areas with the maximum levels are slightly narrower based on the tailored Green's functions. In the frequency bands $f = 4000$ Hz and $f = 5000$ Hz, the dynamic range of the levels with tailored Green's functions is lower than with free-field Green's functions.

5.2 Summary and discussion of the results

This section has shown that the RoBeaT method also works for sound source localization on fans. By using tailored Green's functions, the sound sources in the lower three frequency bands are more clearly identified than with free-field steering vectors. The improvement in spatial resolution corresponds to the findings in the previous section 4, according to which the main lobe widths have been reduced with tailored Green's functions.

The lack of improvement in the results at the higher frequencies also corresponds to the findings from chapter 4. Possible reasons for this, in addition to unsuitable PSF and geometric inaccuracies in the real measurement setup, are the flow around the fan and the unknown directional characteristic of the aeroacoustic sound sources. Green's functions are calculated for monopole sources in a stationary medium both for free-field propagation and tailored by BEM. However, due to the consideration of reflections in the BEM, it can be assumed that deviating directional characteristics have a greater influence on the quality of the results when using tailored Green's functions.

6 CONCLUSIONS

In this paper, the RoBeaT method for rotating sound source localization under consideration of real sound propagation conditions has been presented. The method has been validated both with synthetic and test bench data from known sound sources and with measurement data from a fan.

The results of the synthetic test case have shown that using the correct tailored Green's functions improves the results of the synthetic measurement data with geometry. However, they do not correspond to the free-field PSF. The reason for this is that additional information is used which is not available when using free-field Green's functions. In the test case shown, this results in the main lobe width being reduced. However, the side lobes are increased, especially at low frequencies. Another finding was that the results with tailored Green's functions show a significantly higher dependence on the steering vector formulation.

In the next step, the RoBeaT method was tested with measurement data from a real, rotating loudspeaker. By using the tailored Green's functions, both the level and the position of the source were reconstructed with higher accuracy than when using free-field Green's functions.

When evaluating the measurement data with a fan in a box, the sound source localization at low frequencies has been improved by using the tailored Green's functions compared to the evaluation with free-field Green's functions. In this frequency range, the simulated, tailored Green's functions reproduce the real propagation conditions sufficiently accurately. At high frequencies, however, the results with free-field beamforming are better.

One possible explanation for this is that the simulated Green's functions no longer sufficiently model reality. For the synthetic test case, the results have also been improved in this frequency range by using the tailored Green's functions. This indicates that the actual beamforming algorithm in the RoBeaT method also works at high frequencies as long as the correct Green's functions are used as input.

In order to improve the accuracy of the tailored Green's functions at high frequencies, these could be determined by measurement. One advantage of the RoBeaT method is that this could be done using a spatially stationary sound source, because stationary Green's functions are used as input for rotating beamforming.

References

- [1] CAE Software and Systems GmbH, Gütersloh. *Datenakquisesystem integriertes Frontend mit 112 Kanälen*. URL <https://www.cae-systems.de/fileadmin/CAEpage/Datenblaetter/datasheet-acoustic-camera-frontend.pdf>.
- [2] R. Dougherty, B. Walker, and D. Sutliff. "Locating and quantifying broadband fan sources using in-duct microphones." In *Proceedings of the 16th AIAA/CEAS aeroacoustics conference*. Stockholm, Sweden, 2010. doi:<https://doi.org/10.2514/6.2010-3736>.
- [3] G. Herold and E. Sarradj. "Microphone array method for the characterization of rotating sound sources in axial fans." *Noise Control Eng. J.*, 63(6), 546–551, 2015. doi:<https://doi.org/10.3397/1/376348>.
- [4] ISO. *ISO 13347-3:2004-08, Industrieventilatoren - Bestimmung der Schallleistungspegel unter genormten Laborbedingungen - Teil 3: Hüllflächenverfahren*. Beuth Verlag, Berlin, 2004.
- [5] M. Lehmann. *Entwicklung eines rotierenden Beamformingverfahrens zur Schallquellenlokalisation mittels maßgeschneiderten Greenschen Funktionen*. Ph.D. thesis, Technische Universität Braunschweig, 2022. doi:[10.24355/DBBS.084-202304050725-0](https://doi.org/10.24355/DBBS.084-202304050725-0).

- [6] M. Lehmann, D. Ernst, M. Schneider, C. Spehr, and M. Lummer. “Beamforming for measurements under disturbed propagation conditions using numerically calculated green’s functions.” *J. Sound Vib.*, 520, 116638, 2022. ISSN 0022-460X. doi:<https://doi.org/10.1016/j.jsv.2021.116638>. URL <https://www.sciencedirect.com/science/article/pii/S0022460X21006453>.
- [7] C. Lewis and P. Joseph. “A focused beamformer technique for separating rotor and stator-based broadband sources.” In *Proceedings of the 12th AIAA/CEAS Aeroacoustics Conference (27th AIAA Aeroacoustics Conference)*. Cambridge, Massachusetts, 2006. doi:<https://doi.org/10.2514/6.2006-2710>.
- [8] C. R. Lowis. *In-duct measurement techniques for the characterisation of broadband aero-engine noise*. Dissertation, University of Southampton, 2007.
- [9] M. Lummer. “Installation: numerical investigation.” *CEAS Aeronaut. J.*, 10, 159–178, 2019. doi:<https://doi.org/10.1007/s13272-019-00382-5>.
- [10] M. Lummer, R. A. Akkermans, C. Richter, C. Präber, and J. Delfs. “Validation of a model for open rotor noise predictions and calculation of shielding effects using a fast BEM.” In *Proceedings of the 19th AIAA/CEAS Aeroacoustics Conference*. Berlin, Germany, 2013. doi:<https://doi.org/10.2514/6.2013-2096>.
- [11] C. Ocker and W. Pannert. “Imaging of broadband noise from rotating sources in uniform axial flow.” *AIAA J.*, 55(4), 1185–1193, 2017. doi:<https://doi.org/10.2514/1.J055309>.
- [12] W. Pannert and C. Maier. “Rotating beamforming–motion–compensation in the frequency domain and application of high-resolution beamforming algorithms.” *J. Sound Vib.*, 333(7), 1899–1912, 2014. doi:[10.1016/j.jsv.2013.11.031](https://doi.org/10.1016/j.jsv.2013.11.031).
- [13] E. Sarradj. “Three-dimensional acoustic source mapping with different beamforming steering vector formulations.” *Adv. Acoust. Vib.*, 2012, 2012. doi:<https://doi.org/10.1155/2012/292695>.
- [14] M. Sauereßig. *Verbesserung und Erweiterung der Referenzschallquelle für Mikrofonarrayvalidierung*. Studienarbeit, Hochschule Ansbach, 2020.
- [15] P. Sijtsma. “Using phased array beamforming to locate broadband noise sources inside a turbofan engine.” Technical Report NLR-TP-2009-689, National Aerospace Laboratory NLR, 2006.
- [16] P. Sijtsma, S. Oerlemans, and H. Holthusen. “Location of rotating sources by phased array measurements.” Technical Report NLR-TP-2001-135, National Aerospace Laboratory NLR, 2001.